Evaluating the Performance of Unmanned Ground Vehicle Water Detection

Arturo Rankin
Jet Propulsion Laboratory
California Institute of Technology
4800 Oak Grove Drive
Pasadena, California 91109
(818) 354-9269
Arturo.Rankin@jpl.nasa.gov

Tonislav Ivanov
Jet Propulsion Laboratory
California Institute of Technology
4800 Oak Grove Drive
Pasadena, California 91109
(818) 354-5070
Tonislav.Ivanov@jpl.nasa.gov

Shane Brennan
Jet Propulsion Laboratory
California Institute of Technology
4800 Oak Grove Drive
Pasadena, California 91109
(818) 393-4146
Shane.Brennan@jpl.nasa.gov

ABSTRACT
Water detection is a critical perception requirement for unmanned ground vehicle (UGV) autonomous navigation over cross-country terrain. Under the Robotics Collaborative Technology Alliances (RCTA) program, the Jet Propulsion Laboratory (JPL) developed a set of water detection algorithms that are used to detect, localize, and avoid water bodies large enough to be a hazard to a UGV. The JPL water detection software performs the detection and localization stages using a forward-looking stereo pair of color cameras. The 3D coordinates of water body surface points are then output to a UGV's autonomous mobility system, which is responsible for planning and executing safe paths. There are three primary methods for evaluating the performance of the water detection software. Evaluations can be performed in image space on the intermediate detection product, in map space on the final localized product, or during autonomous navigation to characterize the avoidance of a variety of water bodies. This paper describes a methodology for performing the first two types of water detection performance evaluations.

Categories and Subject Descriptors
OpenGL, GIMP.

General Terms
Algorithms, experimentation, performance.

Keywords
Water detection, ground truth, stereo vision, passive perception.

1. INTRODUCTION
Detecting water hazards is a significant challenge to unmanned ground vehicle (UGV) autonomous navigation over cross country terrain. Traversing through deep water bodies could cause costly damage to the electronics of UGVs. Moreover, a UGV that either breaks down due to water damage or becomes stuck in a water body during an autonomous military mission could cause further complications. These include the shifting of critical resources away from the primary mission to a rescue mission, the placing of soldiers into harm's way to support a rescue mission, the loss of advanced technology to an enemy, and mission failure.

Under the Robotics Collaborative Technology Alliances (RCTA) program, several researchers developed methods for water detection under the advanced perception technology thrust [1][2][3][4][5][6][7]. The Jet Propulsion Laboratory (JPL) participated in this effort, focusing primarily on the cues for water that can be exploited from a stereo pair of color cameras mounted to the front of a UGV. Early in the program, JPL developed an all-purpose multi-cue water detector that uses a rule base to combine water cues from color, texture, and object reflections (detectable in stereo range data) [4]. Subsequently, JPL developed three specialized stand-alone water detection algorithms (also using a forward-looking stereo pair of color cameras) to handle three general scenarios: water bodies in cluttered environments that are reflecting objects in the background (such as trees), water bodies that are out in the open and far away (where reflections of the sky dominate), and water bodies out in the open and close to the UGV (where the color coming out of the water body dominates) [6]. A summary of JPL's four water detectors is in [7].

All four water detection algorithms operate within image space during autonomous navigation and the results are fused into a single terrain classification image. Stereo range data is then used to localize detected water in a digital terrain map [5]. The 3D coordinates of water body map cells are then output to a UGV's autonomous mobility system, which is responsible for planning and executing safe paths.

There are three primary ways to evaluate the performance of the JPL water detection software. Evaluations can be performed in image space on the intermediate detection product, in map space on the final localized product, or during autonomous navigation to characterize how well detected, localized water bodies are avoided. The first two types of performance evaluations are unit-level since they characterize a single subsystem (i.e., the water detection subsystem). The last type of performance evaluation is system-level since it characterizes the combined water detection subsystem and a UGV's response to its output. All three

PerMIS'10, September 28–30, 2010, Baltimore, MD, USA.

evaluation methods have been utilized during the RCTA program. At the close of the RCTA program, the Army Research Laboratory (ARL) designed and executed a system-level experiment to test the avoidance of hazardous terrain (including water bodies) during autonomous navigation [8]. The portion of the experiment that included water body avoidance was performed on experimental unmanned vehicles (XUVs) at Fort Indiantown Gap (FITG), PA. Figure 1 shows an XUV and highlights the sensors used for water detection.

ARL has already published several papers that describe how system-level hazard avoidance evaluations were performed during RCTA [8][9]. In this paper, we focus on unit-level performance evaluations. We describe a methodology for conducting water detection performance evaluations in image space and water localization performance evaluations in map space.

Figure 1. JPL water detection software has been integrated onboard XUVs and evaluated at Ft. Indiantown Gap, PA. A forward-looking stereo pair of color cameras provides water cues from color, texture, and object reflections.

2. EVALUATION IN IMAGE SPACE

2.1 Ground Truthing Water Regions

The JPL water detection software detects water in image space. Therefore, the ideal place to evaluate the performance of JPL water detection is in image space. A formal evaluation of a terrain classifier is typically performed by accurately specifying the pixels that belong to the class of interest and generating a Receiver Operating Characteristic (ROC) curve which plots the true positive classification rate against the false positive classification rate.

In the past, ground truthing water pixels for image sequences (potentially containing hundreds of images) has been a very tedious process. In each image in a sequence, the perimeter of a water body was manually segmented by moving the mouse cursor around the water perimeter and "clicking" (i.e., selecting) a limited number of vertices. The vertices were then connected with straight lines and all the pixels within these N-sided polygons were labeled water. However, since water bodies are not constrained to follow straight lines, there is some inherent ground truth error with this method. Increasing the number of vertices around the perimeter of a water body will reduce the error but will also increase the time required to manually ground truth a sequence. Since the boundary of a water body expands in image space as it is approached, new vertices needed to be selected for each subsequent frame.

To automate the process of ground truthing water bodies in sequences of images, JPL has developed a software tool using Open Graphics Library (OpenGL). In the first image of a sequence, vertices still need to be manually selected. But in each subsequent image, their 2D image coordinates are automatically updated. In the first frame, since we know the surface of a water body is horizontal, we estimate the elevation of a water body by averaging the elevation of each selected vertex using stereo range data. Given the 2D image coordinates of a vertex, it is trivial to look up its 3D coordinates since a left rectified image is registered with the corresponding stereo range image. The stereo correlator may fail to produce disparity data for some of the vertices. For vertices that have stereo 3D coordinates, their vectors are scaled so that they terminate in the estimated water surface plane. For vertices that have no stereo 3D coordinates, a left CAHV camera model [10] is used to modify the rays extending from the vertex pixels so that they also terminate in the estimated water surface plane. The new 3D coordinates of each vertex are recorded for use in subsequent frames. Each time a vertex is modified or added, the corresponding 3D coordinates are generated using the above procedure.

Since UGV position (x, y, z) and orientation data (roll, pitch, yaw) are recorded for each frame in a data set, the 3D coordinates of each vertex can be expressed in a gravity-based world coordinate frame. Given the motion of the UGV from one frame to the next, the left CAHV camera model is transformed and used to perform a linear mapping between the 3D world coordinates of the vertices and their 2D image coordinates. Since the perimeter of a water body typically has texture in visible imagery, it is unlikely that the stereo correlator would fail to produce disparity data for all vertex image coordinates. We currently do not attempt to filter out noisy stereo range measurements from the water body elevation estimate, but a random sample consensus (RANSAC) algorithm could be incorporated to do this.

Figure 2 illustrates the vertex selection process in the first frame of a sequence. Here, a large number of vertices were selected and neighbor vertices were connected with lines to label the water body. The "Action" and "View" drop down menus are shown to illustrate some of the options available to the user. Vertices can be added, moved, or deleted, and entire polygons can be moved or deleted. In addition, vertices and labeled water regions can be saved to file on a frame-by-frame basis and subsequently loaded from file to play back the results, or to further refine the labeling.

Vehicle motion causes the image coordinates of vertices along the perimeter of a water body to change. For example, as a water body is approached, it appears larger in image space. Figure 3 shows a sample result of automatically updating the image coordinates of the perimeter vertices after 47 frames of XUV motion towards the water body. The top row contains the left color image, the right color image, and the stereo range image for frame 0. The middle row contains the same images for frame 46. The bottom image contains a stereo point cloud for frame 46. Stereo was performed at full image resolution (1024x768 pixels). The ground truth region is overlaid on the left images and the stereo point cloud in yellow. In the stereo point cloud, the orange and white areas indicate where there is ground truthing error.

We implemented the following three strategies to help minimize ground truthing error:

1) Allow the user to step through the sequence, pausing at every frame and verifying accurate labeling. If the model of the perimeter is poor, allow the user to move, add, or delete vertices.

2) Provide the option of processing the sequence in reverse order from the final image to the first image. In most of our RCTA sequences, a water body is approached from a distance and the final image contains the greatest perimeter detail. This may not be ideal for all sequences, however. In the final frame of some sequences, portions of a water body fall outside of the cameras field of view. When that occurs, additional vertices may need to be manually added as more of the water body comes into the field of view.
3) Perform non-linear segmentation between vertices to improve the modeling of the water body perimeter.

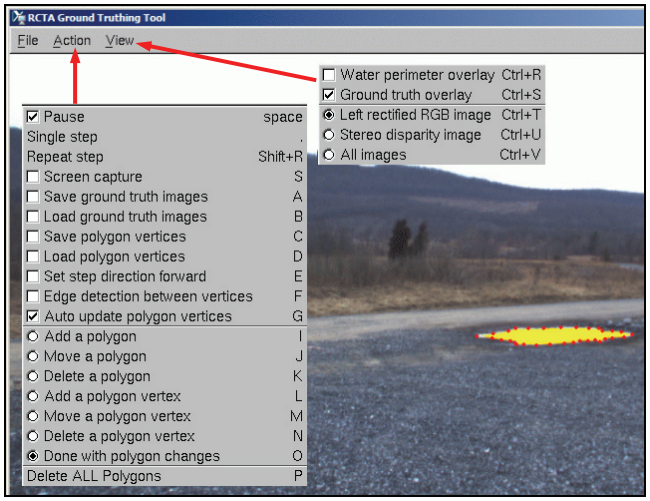

Figure 2. A software tool has been developed to automate the process of ground truthing water bodies in sequences of images. In the first image of a sequence, vertices around the perimeter of water bodies are selected. In this example, the water body is labeled by connecting neighboring vertices with lines. Vertex selection is performed on rectified, full resolution (1024x768 pixels) imagery. Here, we are only showing a portion of the first image. The full image is shown (at a lower resolution) in the upper left image of Figure 3.

The algorithm we selected for non-linear segmentation is called *intelligent scissors* [11]. This algorithm attempts to find the most grayscale contrast closed-loop boundary (Laplacian zero-crossing) while keeping the boundary edge smooth (gradient direction) and the texture around the boundary consistent (gradient magnitude). An optimal graph search called *live-wire boundary* is performed based on Dijkstra's [12] path finding algorithm to find a minimal cost path via dynamic programming. The open-source code for *intelligent scissors*, available under GNU Image Manipulation Program (GIMP), was adapted and integrated into the water body ground truthing tool.

For each frame in an image sequence, this code uses the automatically updated vertices from the water region segmented in the previous frame. We step around the ordered vertex list for each water body and run *intelligent scissors* between each vertex pair. *Intelligent scissors* outputs a set of connected pixels between neighbor vertices. Figure 4 illustrates the advantage of using *intelligent scissors* to model the water perimeter between vertices. In this example, only five vertices were needed along a section of the water boundary that has a length in excess of 20 meters.

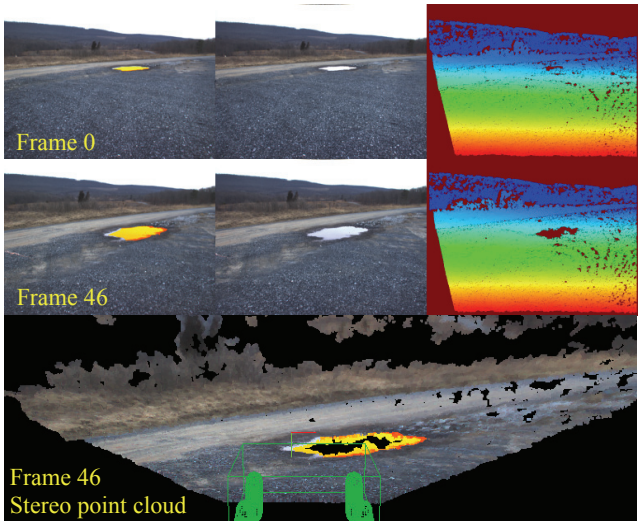

Figure 3. Sample result of automatically updating the image coordinates of the vertices selected in Figure 2 after 47 frames. The top row contains the left rectified image, the right color image, and the stereo range image for frame 0. The middle row contains the same images for frame 46. The bottom image contains a stereo point cloud for frame 46. The ground truth region is overlaid on the left rectified images and the stereo point cloud in yellow. In the color-coded stereo range images, red corresponds to close range, blue corresponds to far range, the colors in between correspond to an intermediate range, and maroon corresponds to no stereo data.

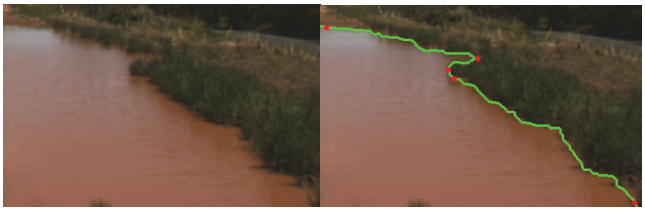

Figure 4. The GIMP image viewer has an intelligent scissors tool to segment image regions along contours. We have extracted the intelligent scissors portion of GIMP and have integrated it into our ground truthing tool. In this example, only 5 vertices were needed along the cropped portion of the water boundary. Intelligent scissors is run for each pair of neighbor vertices to segment the water's edge.

Thus far, we used the JPL water body ground truthing software tool to label one color stereo sequence of images collected at FITG on May 13, 2008. The sequence was collected while an XUV was teleoperated toward the water body partly shown in Figure 4. There is a single large water body at least partially visible in all 143 frames of the sequence. Since terrain classification and stereo range images are registered with the corresponding left camera image (after rectification), only the left rectified images are ground truthed. A binary ground truth image is saved for each left rectified image in the sequence. Figure 5 shows the results of labeling the water body in the first and last

frame in the sequence. The labeling is quite good, but it is not perfect. As illustrated in the bottom row of Figure 5, it does not exclude interior objects extending out of a water body, such as sediment, vegetation, or rocks.

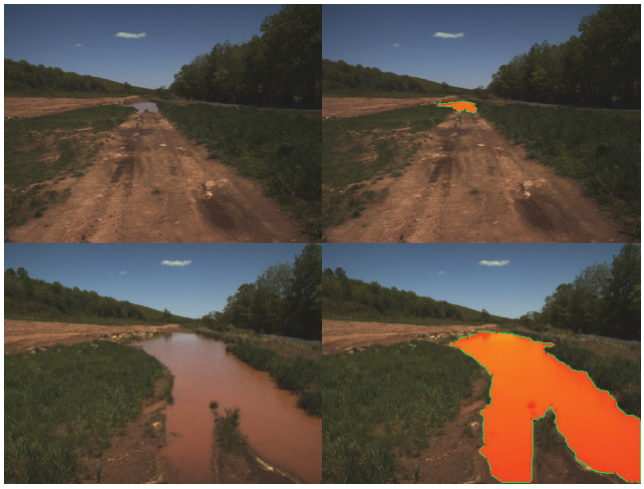

Figure 5. The water perimeter (green) and labeled water region (orange) for the first and last frame of a 143 frame sequence. This sequence was ground truthed using our software tool. The labeling is quite good, but it is not perfect. For example, it does not exclude interior objects extending out of the water.

2.2 Characterizing Detection Performance

The labeled sequence described in Figure 5 was processed off-line with the JPL water detection software with all three specialized detectors enabled. The water body was detected in every frame. Figure 6 shows water detection results in the form of overlapping water cues for the first and last frame in the sequence. The pixels labeled blue, magenta, and red indicate where the water body was detected by one, two, or three water detectors, respectively. The blue regions were detected based on the variation in color, the magenta regions were detected based on the variation in color and sky reflections, and the red regions were detected based on the variation in color, sky reflections, and terrain reflections.

Figure 7 shows water detection results overlaid on the labeled water body for the first and last frame in the sequence. The blue, red, and green pixels indicate true positive detection, false negative detection, and false positive detection, respectively. Note that detector labels almost the entire water body but tends to miss small portions of water on the perimeter. Along the right side of the water body, the missed detection is due to weak reflections of the grass lining the water's edge.

Figure 8 contains a graph of the true positive and false positive water detection rates for each frame in the ground truthed water sequence as a function of the minimum range to the water's leading edge. The true positive detection rate is calculated as the number of pixels correctly classified as water divided by the number of ground truth water pixels. The false positive detection rate is calculated as the number of pixels incorrectly classified as water divided by the number of ground truth water pixels.

Overall, the true positive detection rate increased as the size of the water body in image space increased. The true positive detection rate ranged from 68% (near the beginning of the sequence) to 90% (near the end of the sequence). Note that the false positive detection rate was consistently low for the sequence. The false positive detection rate was 3.3% in one frame but remained below 0.8% in the rest of the frames. Because the false positive detection rate was fairly constant for the entire sequence, we chose the plot format in Figure 8 instead of the standard ROC format. False positive water detection only occurred around the perimeter of the labeled water body. There was substantially less false positive water detection around the perimeter of the labeled water body than false negative water detection.

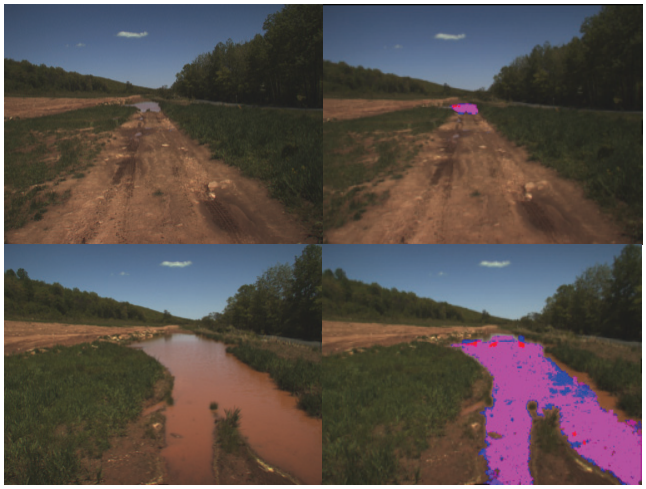

Figure 6. Overlapping water cues for the first and last frame in the ground truthed sequence. The pixels labeled blue, magenta, and red indicate where the water body was detected by one, two, or three water detectors, respectively. The blue regions were detected based on variation in color, the magenta regions were detected based on the variation in color and sky reflections, and the red regions were detected based on the variation in color, sky reflections, and terrain reflections.

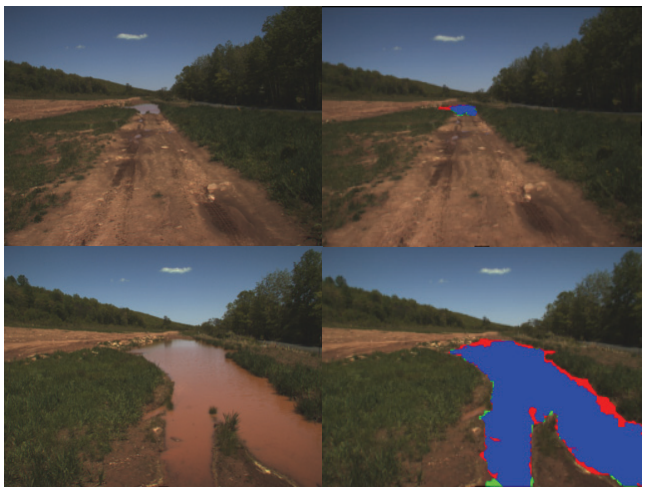

Figure 7. Water detection results for the first and last image in the sequence. The blue, red, and green pixels indicate true positive detection, false negative detection, and false positive detection, respectively.

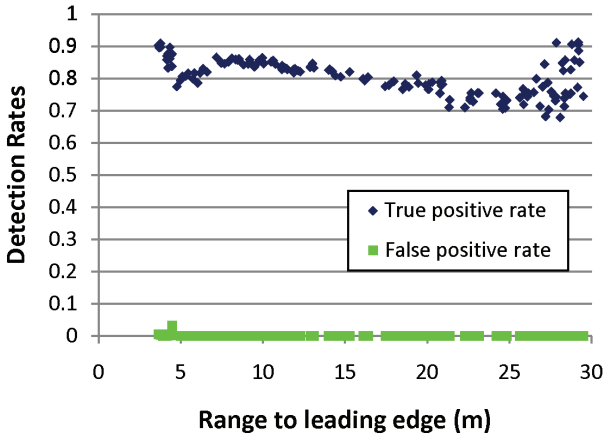

Figure 8. The true and false positive detection rates for each frame in the ground truthed water sequence as a function of the minimum range to the water's leading edge. Each marker corresponds to an image frame.

3. EVALUATION IN MAP SPACE

3.1 Ground Truthing Water Regions

The JPL water detection software localizes detected water in a terrain map. Therefore, the ideal place to evaluate the performance of water body localization is in map space. In order to test the accuracy of water body localization, ground truth 3D coordinates of a water body's perimeter is needed in the same coordinate frame that the vehicle's position is expressed. Ground truth water body measurements can be obtained by tracing the water's perimeter with a positioning sensor, such as differential global positioning system (DGPS), or by surveying fiducials around the water's perimeter with a total station (or other surveying instrument). The location of detected water bodies can then be compared to the ground truth data to determine its accuracy.

Stereo range data is used by the JPL water detection software to localize detected water. Stereo range data around the perimeter of a detected water body is averaged to estimate the elevation of the water body. We don't use the stereo range data corresponding to the surface of detected water bodies for two reasons. First, there may be little or no stereo range data on a water body since the surface of water bodies tend to lack texture, particularly when they are stationary. Secondly, stereo range data on reflections of objects in water has a range that corresponds to the range to the reflected object, not the surface of the water body.

Once the elevation of detected water bodies is estimated, the 3D coordinates (in the stereo range image) of the pixels classified as water are modified to correspond to the surface of water bodies. This modified 3D data are used to label cells in a terrain map as water cells for comparison against the ground truth measurements. As a water body is approached, the estimate of its elevation improves. Temporal filtering is performed in the terrain map to relocate previously detected water [5].

Water localization experiments can be performed on a ground truthed test site with or without the vehicle constrained to a predefined path. During RCTA, one of the test sites used to evaluate water localization constrained the vehicle path by using a General Dynamics Robotic Systems (GDRS) instrumented train.

The instrumented train contained a General Electric 24 volt DC motor, an Ogura Fail-Safe brake, an inertial measurement unit (IMU), a GPS receiver, three color cameras that provided narrow baseline (9.5cm), mid baseline (20.5cm), and wide baseline (30cm) stereo ranging, a GDRS ladar, and the same autonomous mobility computing hardware used on XUVs. Data from the IMU and GPS were combined with a Kalman filter to provide continuous, smoothed absolute positioning data accurate to within 0.5% of the distance traveled [13].

The instrument train was constructed to enable multiple RCTA researchers to evaluate their terrain classification algorithms in a controlled environment. The use of train tracks ensures the perception sensors always follow the same route for each test run. This type of experiment enables one to directly compare the results of multiple test runs where single or multiple factors may be varied each run, such as train speed, time of day (to evaluate the effects of lighting), and the day of year (to evaluate the effects of different environmental conditions).

Perception sensor and navigation data can be logged during test runs for offline processing with terrain classification algorithms, or terrain classification can be performed in real-time and its results logged. Figure 9 contains a picture of the instrumented train and two man-made water bodies (each approximately 1.5m x 2m) constructed adjacent to train tracks at GDRS, Westminster, Maryland. The length of the train tracks at this test site was 171 meters. JPL performed stereo data collections on this course at speed of 1, 3, and 5 m/s.

Figure 9. A JPL passive perception system was mounted to a GDRS instrumented train. Color stereo imagery was collected on a surveyed obstacle course containing two rectangular man-made water bodies at speeds of 1, 3, and 5 m/s.

The corners of the rectangular water bodies were surveyed using a NovAtel OEM4-G2 GPS receiver operating in RT-2 differential mode (with a base station less than 30 meters from the train starting point). The accuracy of this DGPS is 1cm +1 part per million (ppm). At the farthest end of the test course, the DPGS error due to the distance from the GPS base station was less than 2mm. At each corner, DGPS data was averaged for 10 minutes, yielding an accuracy of 1cm circular error probable (CEP), i.e., half of all the data were within 1cm of the ground truth. The standard deviation in both latitude and longitude directions was less than 1cm. DGPS land survey accuracy was verified with a

Leica TCR307 total station on six key points on the train rails. Figure 10 illustrates water detection for one frame during a 1m/s run. Note in the stereo range image that there is no range data on much of the water body, except where there is a reflection of the pole directly behind the water body.

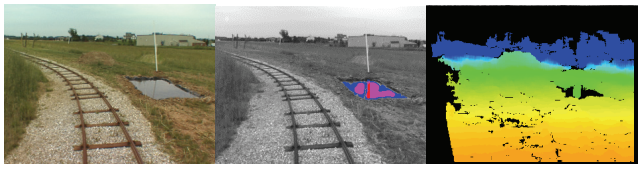

Figure 10. A frame showing the first man-made water body on the test course described in Figure 9 during a 1m/s run (left), water detection results overlaid on a grayscale intensity image (middle), and a wide-baseline stereo range image (right). In the color coded water detection overlay, blue, magenta, and red correspond to one, two, and three cues for water, respectively. In the stereo range image, black corresponds to no range data.

3.2 Characterizing Detection Performance

The 3D coordinates of a water body localized with JPL's water detection software can be compared with the ground truth water body perimeter measurements to produce several measures of accuracy:

1) Difference in the detected and ground truth water body centroid (units: meters).
2) Percentage of the detected water body within the ground truth water body.
3) Percentage of the detected water body outside of the ground truth water body.
4) Percentage of the ground truth water body detected as water.
5) Maximum distance the detected water body perimeter strays from the ground truth water body perimeter (units: meters).

Thus far, GDRS has provided JPL with only the ground truth measurement of a single corner of the second man-made water body. JPL has processed the wide-baseline data from the 1m/s run off-line at an image resolution of 320x240 pixels using the all-purpose multi-cue based water detection algorithm [4]. (This analysis was performed before the specialized water detectors were implemented.) In Figure 11, the upper graph shows the detection and localization of both water bodies and the lower graph shows a zoom-in of the second water body. Using a 20cm resolution terrain map, the JPL water detection software localized the corner of the second man-made water body within 16cm of the ground truth position [13].

Figure 12 contains graphs of the detection range and strength of detection for both water bodies. The first water body was detected at a maximum range of 13.6 meters and the second water body was detected at a maximum range of 10.2 meters. The maximum range of detection for the second water body was slightly lower because elevated terrain near the leading edge occluded a portion of the water.

4. CONCLUSIONS

In this paper, we described a methodology for conducting water detection performance evaluations in image space, and water localization performance evaluations in map space. JPL has developed a software tool for ground truthing water bodies in stereo image sequences. The ground truthing tool enables users to step though a sequence of images and select a limited number of vertices (in left rectified images) around the perimeter of water bodies. We have extracted the *intelligent scissors* portion of GIMP and have integrated it into our ground truthing tool. *Intelligent scissors* is run for each pair of neighbor vertices to segment the water's edge. Stereo vision is used to update the 2D image coordinates of the vertices as the user steps from one frame to the next. At each frame, the user can add, move, or delete vertices, or move or delete entire polygons.

Typically, a water body is ground truthed in image space starting with the final image (where the water body is the largest) and ending with the first image (where the water body is the smallest). Thus far, we have used the JPL water body ground truthing software to label one color stereo sequence of images. In the 143 frame sequence, the water body was detected in every frame. The true positive detection rate ranged from 68% (at a range of 28 meters to the leading edge) to 90% (at a range of 4 meters to the leading edge). The false positive detection rate was 3.3% in one frame but remained below 0.8% in the rest of the frames.

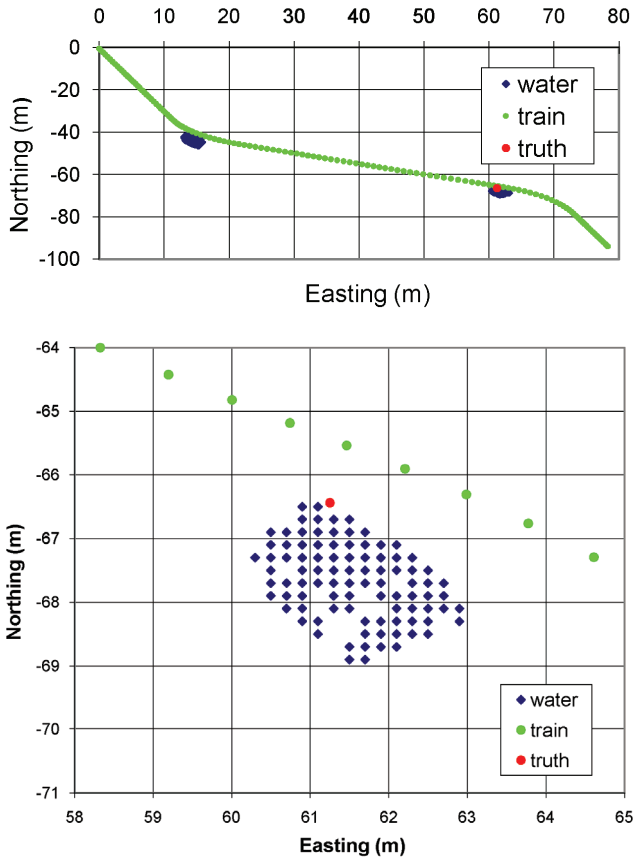

Figure 11. Detection and localization of the two rectangular man-made water bodies shown in Figure 9. The lower graph shows a zoom-in of the second water body. The blue markers are placed at the centers of terrain map cells classified as water.

This evaluation indicated that weak reflections of vegetation lining the edge of a water body are consistently undetected by the three specialized water detectors. In addition, the true positive water detection rate is currently underestimated when there are objects extending out of the interior of a water body, such as sediment, rocks, and vegetation. The reason for this is the water body ground truthing tool does not currently exclude these regions. Additional work is needed to enable the ground truthing tool to exclude these regions, and to filter noisy stereo range measurement during water body elevation estimation.

We also outlined several measures of accuracy for comparing the 3D coordinates of a water body localized with JPL's water detection software with 3D ground truth water body perimeter measurements. We have not experimented with any of these measures yet due to a lack of 3D ground truth water body perimeter measurements to date. More work is needed to determine the usefulness of these measures.

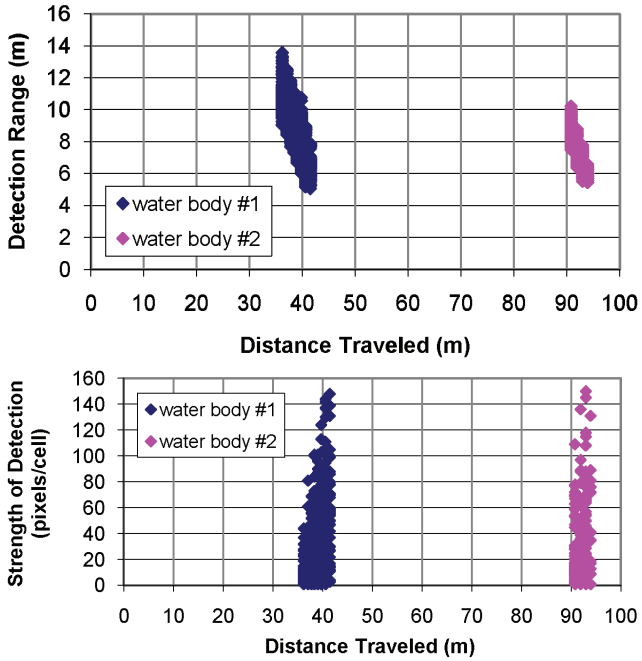

Figure 12. Detection range and strength of detection as a function of distance traveled for the two rectangular man-made water bodies shown in Figure 9.

5. ACKNOWLEDGMENTS

The research described in this paper was carried out by the Jet Propulsion Laboratory, California Institute of Technology, and was sponsored by the U.S. Army under the Robotics Collaborative Technology Alliances and Future Combat System Autonomous Navigation System programs, through agreements with the National Aeronautics and Space Administration (NASA). Reference herein to any specific commercial product, process, or service by trademark, manufacturer, or otherwise, does not constitute or imply its endorsement by the United States Government or the Jet Propulsion Laboratory, California Institute of Technology.

6. REFERENCES

[1] Hong, T., Rasmussen, C., Chang, T., and Shneier, M. 2002. Fusing ladar and color image information for mobile robot feature detection and tracking, *7th International Conference on Intelligent Autonomous Systems*, (Marina Del Ray, CA, Mar. 2002).

[2] Matthies, L., Bellutta, P., and McHenry, M. 2003. Detecting water hazards for autonomous off-road navigation. *Proceedings of SPIE*, Vol. 5083 (Orlando, FL, Apr. 2003), 231-242.

[3] Sarwal, A., Nett, J., and Simon, D. 2004. Detection of small water bodies. *PercepTek Robotics Technical Report*, Littleton, CO, (http://www.dtic.mil, AD# ADA433004).

[4] Rankin, A., Matthies, L., and Huertas, A. 2004. Daytime water detection by fusing multiple cues for autonomous off-road navigation. *Proceedings of the 24th Army Science Conference*, (Orlando, FL, Nov. 2004).

[5] Rankin, A. and Matthies, L. 2006. Daytime water detection and localization for unmanned vehicle autonomous navigation. *Proceedings of the 25th Army Science Conference*, (Orlando, FL, Nov. 2006).

[6] Rankin, A. and Matthies, L. 2010. Daytime water detection based on color variation. *To appear in: Proceedings of the IEEE/RSJ International Conference on Intelligent Robots and Systems*, (Taipei, Taiwan, Oct. 2010).

[7] Rankin, A., Bajracharya, M., Huertas, A., Howard, A., Moghaddam, B., Brennan, S., Ansar, A., Tang, B., Turmon, M., and Matthies, L. 2010. Stereo-vision based perception capabilities developed during the Robotics Collaborative Technology Alliances program. *Proceedings of SPIE*, Vol. 7692, (Orlando, FL, Apr. 2010), 76920C1-76920C15.

[8] Bodt, B., Childers, M., and Camden, R. 2010. A capstone experiment to assess unmanned ground vehicle tactical behaviors developed under the robotics collaborative technology alliance. *Proceedings of AUVSI*, (Denver, CO, Aug. 2010).

[9] Bodt, B. and Childers, M. 2010. A place at the table: the role of formal experimentation in the robotics collaborative technology alliance. *Proceedings of the 78th MORS Symposium*, (Quantico, VA, Jun. 2010).

[10] Yakimovsky, Y. and Cunningham, R. 1978. A system for extracting three-dimensional measurements from a stereo pair of TV cameras. *Computer Graphics and Image Processing*, 7, 195-210.

[11] Mortensen, E.N. and Barrett, W.A. 1995. Intelligent scissors for image composition. *International Conference on Computer Graphics and Interactive Techniques*, Los Angeles, CA, Aug. 1995), 191-198.

[12] Dijkstra, E.W. 1959. A note on two problems in connection with graphs, *Numerische Mathematik*, Vol. 1, 269-271.

[13] Rankin, A., Huertas, A., and Matthies, L. 2005. Evaluation of stereo vision obstacle detection algorithms for off-road autonomous navigation. *Proceedings of AUVSI*, (Baltimore, MD, Jun. 2005).